

Water isotopes in the GISS ModelE land surface scheme

I. Aleinov*, G.A. Schmidt

NASA Goddard Institute for Space Studies, 2880 Broadway, New York, NY 10025, United States

Center for Climate Systems Research, Columbia University, 2880 Broadway, New York, NY 10025, United States

Received 18 July 2005; accepted 20 December 2005

Available online 24 March 2006

Abstract

We describe the isotope-capable Land Surface Model (LSM) developed at NASA Goddard Institute for Space Studies (GISS). This model is a part of the GISS ModelE General Circulation Model (GCM), which includes the water isotopes H_2^{18}O and HDO as tracers in every aspect of the model's hydrological cycle. We discuss results for the soil isotopes from a number of full GCM simulations. In particular, we focus upon the spin up and equilibrium behavior of the isotope fields in a present day (ca. 1980) control simulation and the response of the isotopes to forcings over transient AMIP-style 20th century simulations. In addition, we investigate whether the isotope fields are affected by a change in the runoff algorithm, and so examine whether the isotope fields have the potential to constrain model land surface physics.

© 2006 Elsevier B.V. All rights reserved.

Keywords: iPILPS; stable water isotopes; land surface model; GCM; GISS ModelE

1. Introduction

The modeling of the land surface and soil moisture is increasingly seen as an important factor in understanding climate change. Thus evaluating hydrological pathways in land surface schemes in climate models and evaluating them against observations is increasingly necessary. Water isotopes are superlative tracers of hydrological processes and are now being incorporated into both off-line land surface modules and General Circulation Models (GCMs). These tracers can potentially help in the evaluation of the model parameterizations as well as diagnose the implications or causes of

any potentially observed changes (Henderson-Sellers et al., 2006-this volume).

The Goddard Institute for Space Studies (GISS) isotope-capable Land Surface Model (LSM) presented here is a part of GISS ModelE GCM version (Schmidt et al., 2006), which includes the water isotopes H_2^{18}O and HDO as tracers in every aspect of the model's hydrological cycle (Schmidt et al., 2005). Previous versions of this model (Jouzel et al., 1991) used a simple bucket scheme for the land surface isotopes (i.e. a simple budget for the isotopes in the soils was kept simply to track the conservation of each species). Such a scheme was inadequate for extensive evaluation of the isotopes against observations. In particular it neglected the vertical gradient of isotope concentration in the soil and didn't take into account different concentrations of isotopes in the soil and in the canopy water. As a result the partition of isotopes between evaporation and runoff was not modeled with great accuracy. The model we

* Corresponding author. Center for Climate Systems Research, Columbia University, 2880 Broadway, New York, NY 10025, United States.

E-mail address: ialeinov@giss.nasa.gov (I. Aleinov).

present here does allow for these factors, and thus can be sensibly used to evaluate the land surface scheme in the model.

A detailed description of GISS modelE is given in Schmidt et al. (2006) and general aspects of the implementation of the isotope tracers in the atmospheric model can be found in Schmidt et al. (2005), but we discuss the implementation in the land surface scheme in more detail below.

We first present the results of full GCM simulations for a present-day (ca. 1980) to look at the spin up properties of the isotope fields and the equilibrium state. The present day study concentrates on time series of hydrological parameters for several geographical spots selected by the iPILPS group (Henderson-Sellers et al., 2006, this volume). Then we compare it to a sensitivity simulation done with a different runoff algorithm. After that we examine a transient AMIP-style 20th Century simulation to investigate possible soil isotope links to climate change.

Throughout the paper we present the amount of isotopes as isotopic ratios $\delta^{18}\text{O}$ and $\delta\text{D}\text{‰}$ (per mil) defined as

$$\delta = 1000 \left(\frac{R_{\text{sample}}}{R_{\text{VSMOW}}} - 1 \right), \quad (1)$$

where R_{sample} is the ratio of the mass of water containing the isotope to the mass of water with principal isotope and R_{VSMOW} is the standard ratio (Vienna Standard Mean Ocean Water). To highlight the difference between the two principle water isotopes, we use the deuterium excess (d-excess) defined as $d = \delta\text{D} - 8\delta^{18}\text{O}$.

2. Land surface model description

GISS Land Surface Model (LSM) is based on the original Rosenzweig and Abramopoulos (1997) model with various additions and improvements. In particular, a three-layer snow model was implemented (Lynch-Stieglitz, 1994), the canopy conductance algorithm was replaced with the one based on plant physiology (Friend and Kiang, 2005), new algorithm for the underground runoff was developed based on the TOPMODEL approach of Beven and Kirkby (1979) and water tracers were incorporated into the model. The GISS LSM consists of three integrated modules: ground hydrology model, snow model and vegetation model. All modules conserve water and energy up to machine accuracy and are capable of keeping track of passive water tracers (HDO and H_2^{18}O in current work). The area of the model

cell is subdivided into two parts corresponding to bare soil and vegetated soil. These parts are treated independently, each part having its own set of prognostic variables. In presence of snow each part has a certain fraction covered by snow.

The thickness of the modeled soil is everywhere 3.5m. It is split into six layers with the thickness of layers (from top to bottom) being 0.1m, 0.17m, 0.30m, 0.51m, 0.89m and 1.53m. We distinguish between five textures of soil: sand, loam, clay, peat and bedrock. Each layer may contain a mixture of these soil types, so all hydraulic and thermodynamic properties of the layer are computed according to their fractions. The state of each layer i is described by two prognostic variables: total amount of water in the layer W_i (m) and heat content of the layer H_i (J m^{-2}) (including latent heat).

The vertical flux of water F_w (m s^{-1}) in the soil is computed according to Darcy's law

$$F_w = -K_w \frac{\partial}{\partial z} (h + z) \quad (2)$$

and the vertical heat flux F_h (W m^{-2}) is assumed to obey the heat transport equation

$$F_h = -K_w \frac{\partial T}{\partial z} + F_w T \rho_w c_w, \quad (3)$$

where z is a vertical coordinate, h is a matric potential, T is the temperature of the layer, K_w and K_h are hydraulic and thermal conductivities, respectively, and ρ_w and c_w are density and specific heat capacity of the water. The boundary at the bottom of the modeled soil is considered impermeable for both water and heat. The boundary conditions at the top of the upper soil layer are obtained as a result of interaction with atmosphere, canopy and snow.

The water balance equation for each layer i includes vertical fluxes at the layer boundaries and sinks due to transpiration E_i and underground runoff R_i

$$\frac{dW_i}{dt} = F_{w_{i+1}} - F_{w_i} - E_i - R_i \quad (4)$$

and for energy balance we have

$$\frac{dH_i}{dt} = F_{h_{i+1}} - F_{h_i} - (E_i + R_i) T_i \rho_w c_w, \quad (5)$$

where T_i is average layer temperature, F_{w_i} and F_{h_i} are fluxes at the upper boundary of the layer i as defined by (2) and (3). The boundary condition at the bottom of the modeled soil yields $F_{w_{\text{bot}}}=0$, $F_{h_{\text{bot}}}=0$. The model has two options to compute the underground runoff. The

“standard” option is based on the average slope s in the cell

$$R_i = K_{wi}s \frac{\Delta Z_i}{\delta}, \quad (6)$$

where ΔZ_i is the thickness of the layer and δ is an average distance between the sinks (see Abramopoulos et al., 1988). The TOPMODEL option uses approach of Beven and Kirkby (1979). The underground runoff for layer i in this case is computed as follows

$$R_i^T = e^{-\lambda_t} K_{wsi} \frac{W_i}{W_{si}} \Delta Z_i, \quad (7)$$

where λ_t is topographic index (as defined in Beven and Kirkby (1979)), K_{wsi} is saturated hydraulic conductivity and W_{si} is water holding capacity at saturation of the layer. Strictly speaking, one can't directly apply the TOPMODEL formulas to the model which is discretized by splitting the soil into a set of horizontal layers. Formula (7) should be considered as an extension of the TOPMODEL approach in a sense that it yields the TOPMODEL formula in a continuous limit when the assumptions of the TOPMODEL approach hold.

The hydraulic conductivity K_w and the matric potential h were approximated by fitting the following function to the observed data

$$f(\theta) = \exp(a_{-1}\theta^{-1} + a_0 + a_1\theta + a_2\theta^2) \quad (8)$$

where $\theta = W_i/\Delta Z_i$ and a_{-1}, \dots, a_2 are fitting constants (see Abramopoulos et al., 1988).

The potential transpiration E_i (m s^{-1}) from the layer i is

$$E_{\text{pot } i} = \beta_i \frac{1}{(C_c^{-1} + C_a^{-1})} \frac{\rho_a}{\rho_w} (q_{\text{sat}} - q_s), \quad (9)$$

where ρ_a and ρ_w are densities of surface air and water, q_s is humidity of surface air and q_{sat} is saturated humidity at canopy temperature. C_c is canopy conductance and $C_a = C_q \nu$ describes turbulent transport, where C_q is a transfer coefficient and ν is wind speed at surface. The coefficients

$$\beta_i = A(1 - f_i^{\text{ice}}) f_i^{\text{root}} \max\left(\frac{h_w - h_i}{h_w}, 0\right) \quad (10)$$

describe the distribution of transpiration over the layers according to fraction of ice f_i^{ice} , root fraction f_i^{root} and matrix potential h_i of the layer. Here h_w is wilting point and coefficient A is chosen in such a way that $\sum \beta_i = 1$.

Actual transpiration is subject to water availability and is computed as

$$E_i = \min\left(E_{\text{pot } i}, \frac{W_i - W_{\text{min } i}}{\Delta t}\right), \quad (11)$$

where $W_{\text{min } i}$ is minimal water storage capacity of the layer and Δt is the time step.

Vegetation is currently modeled as a single layer on top of the soil with its own prognostic variables W_c for water and H_c for heat content. W_c is the water accumulated on leaves as a result of precipitation and dew, it doesn't include stem water which is ignored in our model. The model currently has eight types of vegetation: tundra, grass, shrub, trees, deciduous forest, evergreen forest, rainforest and crops. Each model cell can have a mixture of different vegetation types described by corresponding areal fractions. All vegetation fractions are fixed through the run and vegetation properties (such as leaf area index, root fraction, albedo, etc.) have a prescribed seasonal variation. The algorithm for precipitation interception by canopy is described in Rosenzweig and Abramopoulos (1997). For canopy conductance we employ the model based on actual plant physiology which was developed by Friend and Kiang (2005).

GISS LSM uses a snow model based on Lynch-Stieglitz (1994). The model consists of three layers of snow which can collapse to one layer for thin snow (thinner than 15 cm). Each layer is described by three prognostic variables: water equivalent W_i (m), heat content H_i (J/m^2) and thickness Z_i (m). On each time step some amount of melt water can move to lower layers and refreeze there or propagate further until it reaches the soil surface and drains out of the snow pack. The total snow fraction is a function of snow depth and topography variance and is computed according to Roesch et al. (2001). The fraction of canopy covered by snow is a function of snow depth and canopy masking depth as defined in Rosenzweig and Abramopoulos (1997).

The surface fluxes are computed similarly to Rosenzweig and Abramopoulos (1997). All the prognostic variables are updated explicitly, except for snow model, where we use an implicit solver for heat transport. A special flux limiting technique is employed when propagating the water in the soil. This technique reduces certain fluxes to make sure that at the end of the time step no layer has more water than is defined by its saturation limit and no layer is depleted below its minimal water storage capacity.

Special care is taken to ensure that water and energy are conserved up to machine accuracy. On each time step

a control routine is called which computes conservation errors and compares them to allowed tolerance (currently set to 10^{-13} m/s for water flux and 10^{-5} W for energy flux). Should it happen that this condition is violated, the program is stopped and the code is examined for programming errors. There were no such events during iPIPLS simulations.

3. Implementation of passive water tracers

For propagation of tracers we use an upstream scheme which employs the same fluxes of water that were used to update the water content of soil layers. The problem with application of such algorithm is that it is not clear what is “upstream” tracer concentration in our case. It is possible that at the beginning of the time step the “upstream” cell has no water at all (and hence undefined tracer concentration) and still there is non-zero water flux from that cell because water comes from the further “upstream” cell.

To deal with this problem we developed the following algorithm. The advection of tracers is performed as a sequence of two “sweeps”: “down” and “up”. The idea is to update water with tracer in such a way that upstream cell always contains water. We start from the upper layer to which we add precipitation and dew. Then we compute the concentration of tracer c_i (kg/m^3) in each layer that contains water

$$c_i = C_i/W_i \quad (12)$$

where C_i is the amount of tracer in the i th layer in kg/m^2 . After that we do a sweep down starting from the top layer and going from top to bottom advecting tracers only at the boundaries where water flux is directed downwards. So, for i from 2 to n if $F_{wi} < 0$ we update the amount of tracer in the following way

$$C_i = C_i - c_{i-1}F_{wi}\Delta t, \quad (13)$$

$$C_{i-1} = C_{i-1} + c_{i-1}F_{wi}\Delta t, \quad (14)$$

$$W_i = W_i - F_{wi}\Delta t, \quad (15)$$

$$W_{i-1} = W_{i-1} + F_{wi}\Delta t, \quad (16)$$

$$c_i = C_i/W_i. \quad (17)$$

The sweep up is then performed in a similar way, starting from $i=n-1$ and ending with $i=1$. After both sweeps are done the water associated with evapotranspiration and runoff is removed and the amount of tracer is updated accordingly. In our algorithm we assume that all

water that comes to the layer immediately mixes with the rest of the layer water so that concentration of tracer inside the layer is always uniform. As a consequence the concentration of tracer in the layer is changed only when the water is added and stays the same when water is removed. This allows some simplifications to the algorithm. In particular, if soil water was already updated elsewhere and steps (13)–(17) are performed only to advect tracers then step (16) can be skipped since after the sweep one will never need the amount of water in the upstream cells.

The algorithm described above is applied separately to the canopy, snow and soil. Separate treatment is possible because the flux of water between these LSM elements is always directed down from canopy to snow and then to soil. So we can use the same approach of updating tracers in the direction of water flow. We start from the canopy (which doesn't need sweeps because it contains only one layer), then process snow and after that treat soil.

The water isotopes tracers are almost completely passive in the land surface scheme, i.e. there is no fractionation at any change of phase in the soil or during runoff. There are two exceptions, however, for the evaporation of water from bare soil and the wet canopy, where the isotopes are assumed to fractionate. Thus depending on the amount of canopy or bare soil

Table 1
Fractions of soil textures in the GCM cells corresponding to iPIPLS sites

Layer	Sand	Loam	Clay	Peat	Rock
<i>Tumbarumba</i>					
1	0.4950	0.1991	0.3059	0.0000	0.0000
2	0.4669	0.1711	0.3620	0.0000	0.0000
3	0.2730	0.1201	0.6070	0.0000	0.0000
4	0.2292	0.1385	0.4982	0.0000	0.1342
5	0.1585	0.1191	0.2442	0.0000	0.4782
6	0.0129	0.0199	0.0666	0.0000	0.9006
<i>Manaus</i>					
1	0.2280	0.1750	0.5970	0.0000	0.0000
2	0.2188	0.1593	0.6219	0.0000	0.0000
3	0.2310	0.1405	0.6286	0.0000	0.0000
4	0.2361	0.1028	0.6610	0.0000	0.0000
5	0.0985	0.0696	0.4481	0.0000	0.3838
6	0.0190	0.0242	0.1298	0.0000	0.8269
<i>Munich</i>					
1	0.1758	0.5810	0.2433	0.0000	0.0000
2	0.1729	0.5810	0.2461	0.0000	0.0000
3	0.1955	0.5530	0.2414	0.0000	0.0101
4	0.2505	0.4476	0.1535	0.0000	0.1484
5	0.0401	0.2067	0.0750	0.0000	0.6782
6	0.0066	0.1665	0.0300	0.0000	0.7969

Table 2

Fractions of vegetation and bare soil in the GCM cells corresponding to iPILPS sites: Tumberumba (1), Manaus (2), Munich (3)

	Tundra	Grass	Shrub	Trees	Deciduous	Evergreen	Rainforest	Crops	Bare soil
1	0.0000	0.0601	0.0000	0.0000	0.0147	0.5392	0.0000	0.0206	0.3654
2	0.0000	0.0000	0.0000	0.0000	0.0000	0.0000	0.9991	0.0009	0.0000
3	0.0000	0.0000	0.0000	0.0000	0.4837	0.2073	0.0000	0.3090	0.0000

evaporation, the soil water would be expected to be slightly more enriched. This allows one in theory to estimate the partitioning of evaporation and transpiration by looking at the difference in isotopic ratios in runoff and precipitation (given the relevant fractionation factor).

Fractionation processes in the rest of the model (during open water evaporation, condensation within clouds, etc.) are described fully in Schmidt et al. (2005). However, for the purposes of this paper, the basic consequences are relatively simple. Evaporation from open water is significantly depleted in heavy isotopes. As temperatures in an air mass cool, or water is progressively rained out, the rainfall (which is more enriched than the water vapor from which it derives) becomes progressively more depleted. In different regions, this process gives rise to different correlations with surface variables, i.e. the isotopic ratio is positively correlated with surface temperature in the mid-latitudes

while it is negatively correlated with precipitation in the tropics.

4. Present day simulations

The present day simulations are performed with boundary conditions and atmospheric composition fixed at ca. 1980 conditions (decadal mean values for the sea surface temperature (SST), sea ice concentrations and aerosol and ozone fields) and correspond to the M20 simulations described in Schmidt et al. (2006). Model resolution was $4^\circ \times 5^\circ$. For soil textures we used the datasets described in Webb et al. (1993, 1991) and Zolber (1986) and the vegetation distribution was prescribed according to Matthews (1983, 1984). These datasets are currently used in all GISS GCM simulations. They were tested in Rosenzweig and Abramopoulos (1997) and Abramopoulos et al. (1988) and produced satisfactory

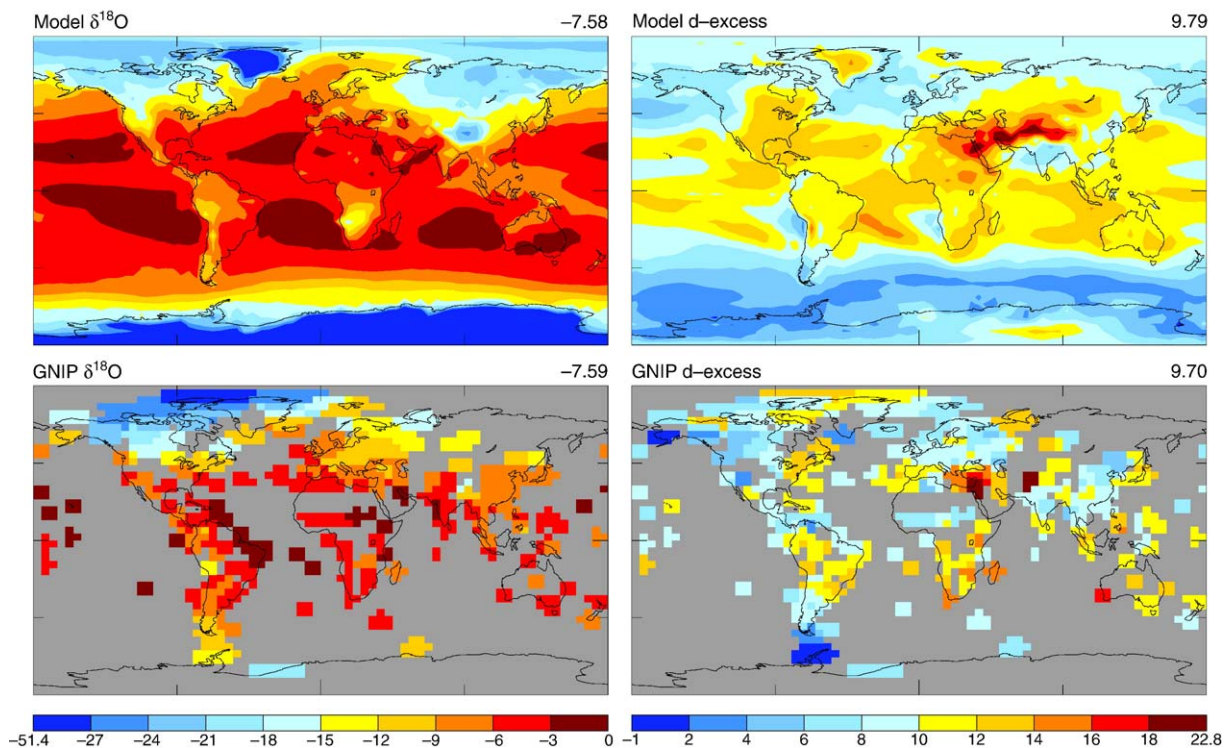


Fig. 1. Annual mean $\delta^{18}\text{O}\text{‰}$ and d-excess ‰ in a control simulation (averaged over last 5 years) and in the GNIP database.

results. For the cells involved in iPILPS experiments these datasets slightly differ from those suggested by iPILPS project, but we decided to leave them as they are in GISS GCM for compatibility with neighboring cells. Also, GISS datasets provide vertical profiles of soil textures while the iPILPS parameters are averaged over the soil depth. Corresponding soil and vegetation parameters are shown in Tables 1 and 2.

For the purpose of investigation of spin-up processes the initial amount of water in soil layers was set to 50% of saturated holding capacity and the isotope ratios were set to VSMOW values ($\delta=0\text{‰}$). The goal of these simulations was to estimate the spin-up time of the model and to study in more detail the behavior of the model at the sites of interest for iPILPS project. The duration of each simulation was 20 years, during which we saved time series of hydrological data for the following sites: wet sclerophyll forest, Tumbarumba, Australia (35°S 148°E), tropical rainforest, Manaus, Brazil (3°S , 60°W) and Mid-latitude grass and wood-

land, Munich (Neuherberg), Germany (48°N 11°E). We will first present the results of control simulation made with the “standard” (6) runoff algorithm, then we will discuss the sensitivity of the model comparing the results of control simulation to those of the simulation made with TOPMODEL (7) runoff algorithm. Further discussion of the control simulation can be found in Henderson-Sellers et al. (2006, this volume).

Though in this paper we mostly concentrate on isotopes in a Land Surface Model, we first check that driving data provided by GCM is adequate for our purposes. In Fig. 1 we compare global annual mean concentrations of isotopes in the precipitation in the control simulation to the data available from the Global Network of Isotopes in Precipitation (GNIP) dataset (IAEA, 2001). The modeled values $\delta^{18}\text{O}$ show a very good agreement with the observations. The modeled d-excess also has a good match, though as a second order parameter it is more sensitive and shows a little more departure from observations.

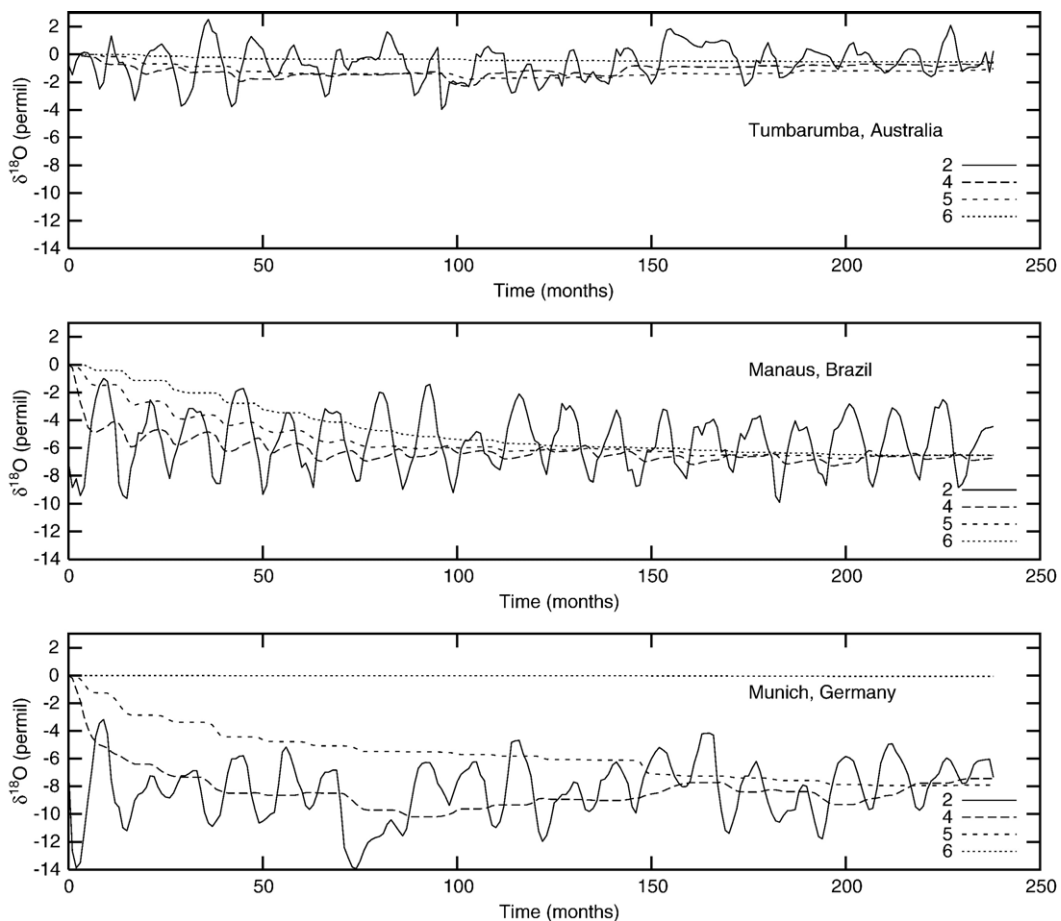


Fig. 2. $\delta^{18}\text{O}\text{‰}$ in soil layers 2, 4, 5 and 6 (monthly means for a 20 years control simulation).

Fig. 2 shows monthly averaged time series for the isotopic ratio $\delta^{18}\text{O}$ in four different layers of soil. One can see that at all three sites the layers four and below have very smooth profile and basically exhibit no seasonal variation. At Amazon rainforest (Manaus) all layers reached equilibrium in about ten years. At Munich and Tumbarumba, on the other hand, though most layers stabilized at approximately the same time, layer 6 didn't change much and may be still quite away from equilibrium. Such behavior is due to specific properties of our ground hydrology model which takes most of the water from upper soil layers for transpiration and runoff, so that little water reaches lower layers unless one has heavy rainstorms (as at Amazon site). This "feature" can be easily seen on Fig. 3, which presents the amount of water in corresponding layers. At Munich and Tumbarumba sites the sixth layer quickly becomes depleted, its water content falls below wilting point and transpiration and runoff from that layer (and replenishment from above) become negligible.

Hydraulic properties depend exponentially on the amount of water in the layer (see (8)). As a result the transition between the layers that actively participate in water exchange and the layers which basically have zero water fluxes has a form of a threshold. So one can assume that distribution of layers is bimodal: the layer either participates in water exchange and reaches equilibrium in 10–15 years or the layer stays mostly passive and needs much longer times to reach equilibrium. Existence of such passive layers may indicate a problem we have in our ground hydrology algorithm. We are planning to address this issue in our future research.

Fig. 4 shows the seasonal cycle of $\delta^{18}\text{O}$ in total runoff and evaporation for the year 20. As one might expect, the concentration of H_2^{18}O in runoff generally is higher than in evaporation due to fractionation at a change of phase during the evaporation from the wet canopy and bare soil. Fig. 5 shows vertical profiles of $\delta^{18}\text{O}$ and d-excess for four different seasons. The sharp kink between layers 5 and 6 at the Munich site indicates that layer 6 hasn't yet reached the equilibrium. A similar

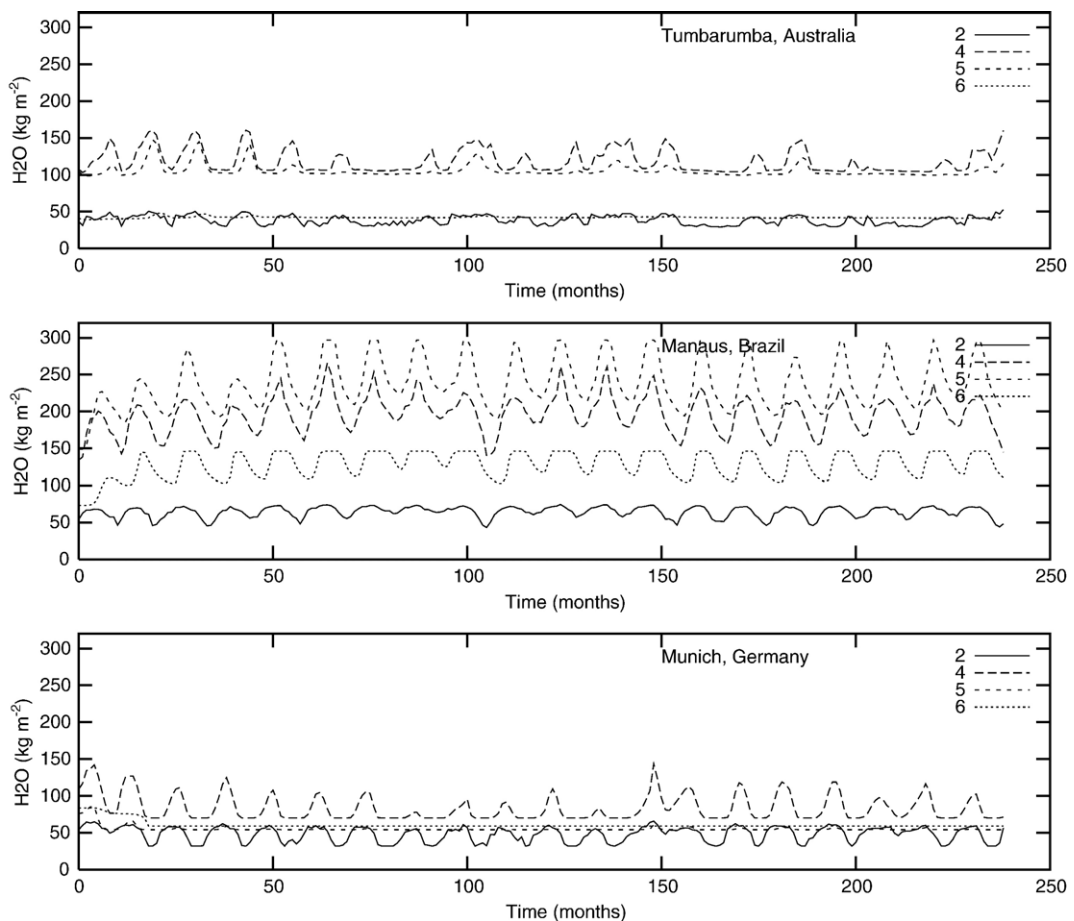


Fig. 3. Soil water (kg m^{-2}) in layers 2, 4, 5 and 6 (monthly means for 20-year control simulation).

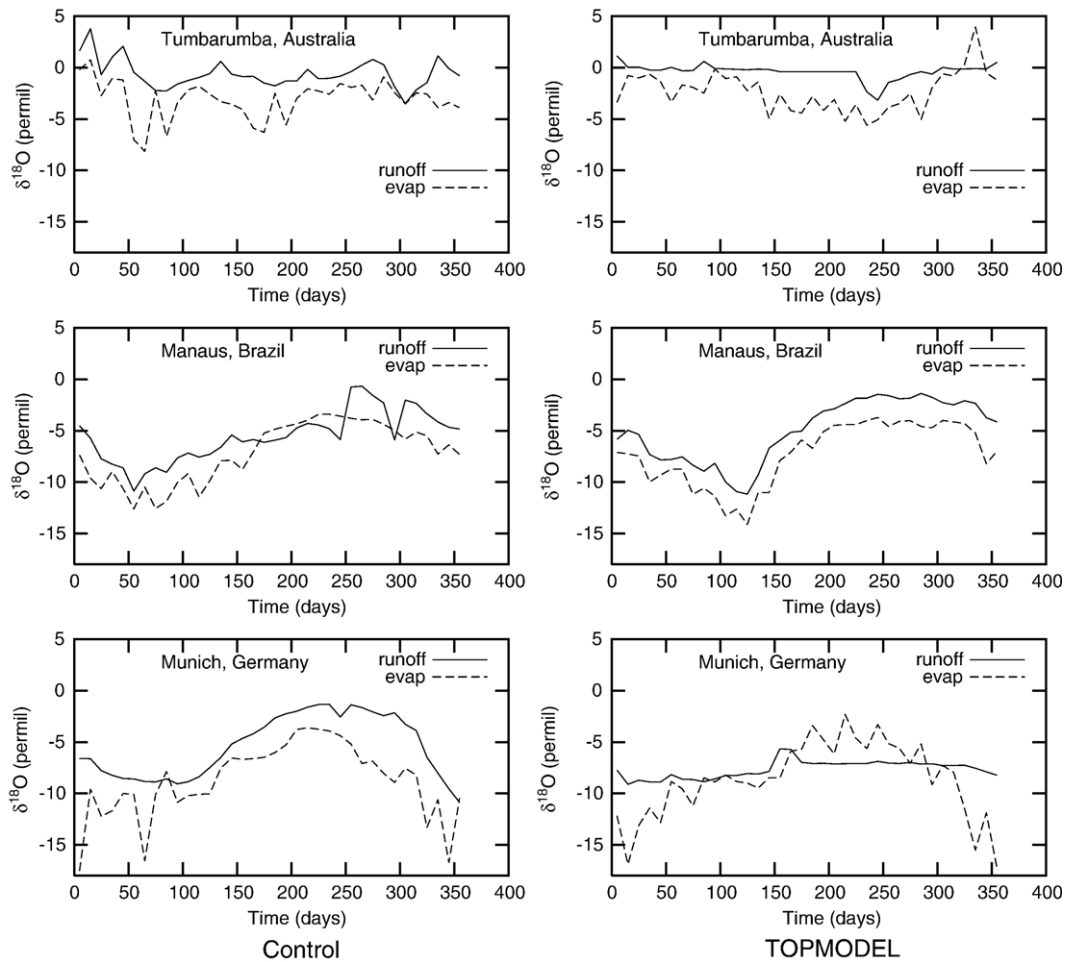


Fig. 4. $\delta^{18}\text{O}\%$ in total runoff and evaporation. The graphs present 10-day averages for the year 20. Left column shows results for control simulation. Right column shows results for the simulation with TOPMODEL runoff.

feature on d-excess graph for Tumberumba most probably means that layer 6 in that region also didn't reach the equilibrium. The results of the simulation made with TOPMODEL runoff algorithm are presented in right columns of Figs. 4 and 5. Though in general the results look similar, there are some noticeable differences. The runoff curves exhibit less variation for TOPMODEL simulation on Fig. 4. Also, structures of vertical profiles look a little different, in particular, on Munich graphs for TOPMODEL algorithms the curve makes sharp turn at level 4 indicating that level 5 is probably still out of equilibrium. Even for Amazon site the curve slightly bends towards zero below layer 5. Hence, we conclude that the TOPMODEL runoff algorithm implies a longer spin-up time.

Table 3 presents river outflow and corresponding $\delta^{18}\text{O}$ at the mouth for river basins which contain investigated regions. Observed outflow is reported

according to Milliman and Meade (1983). Observations of $\delta^{18}\text{O}$ were obtained from Stichler and Schotterer (2000) (Danube), Gibson et al. (2002) (Amazon) and Simpson and Herczeg (1991) (Murray). There is some discrepancy in total river outflow though the isotope ratios, on the other hand, are quite close to observations. The second value in each column corresponds to the TOPMODEL simulation. The values of $\delta^{18}\text{O}$ are close in both simulations, though there is a tendency for the values of TOPMODEL simulation to be a little lower.

The errors in the outflow for Murray and Amazon are mainly due to excess or deficit of precipitation at certain regions in the ModelE GCM (which is a known problem). The fact that we are getting correct isotope concentrations in spite of outflow errors indicates that isotope concentrations are not very sensitive to the amount of precipitation in these areas, provided that

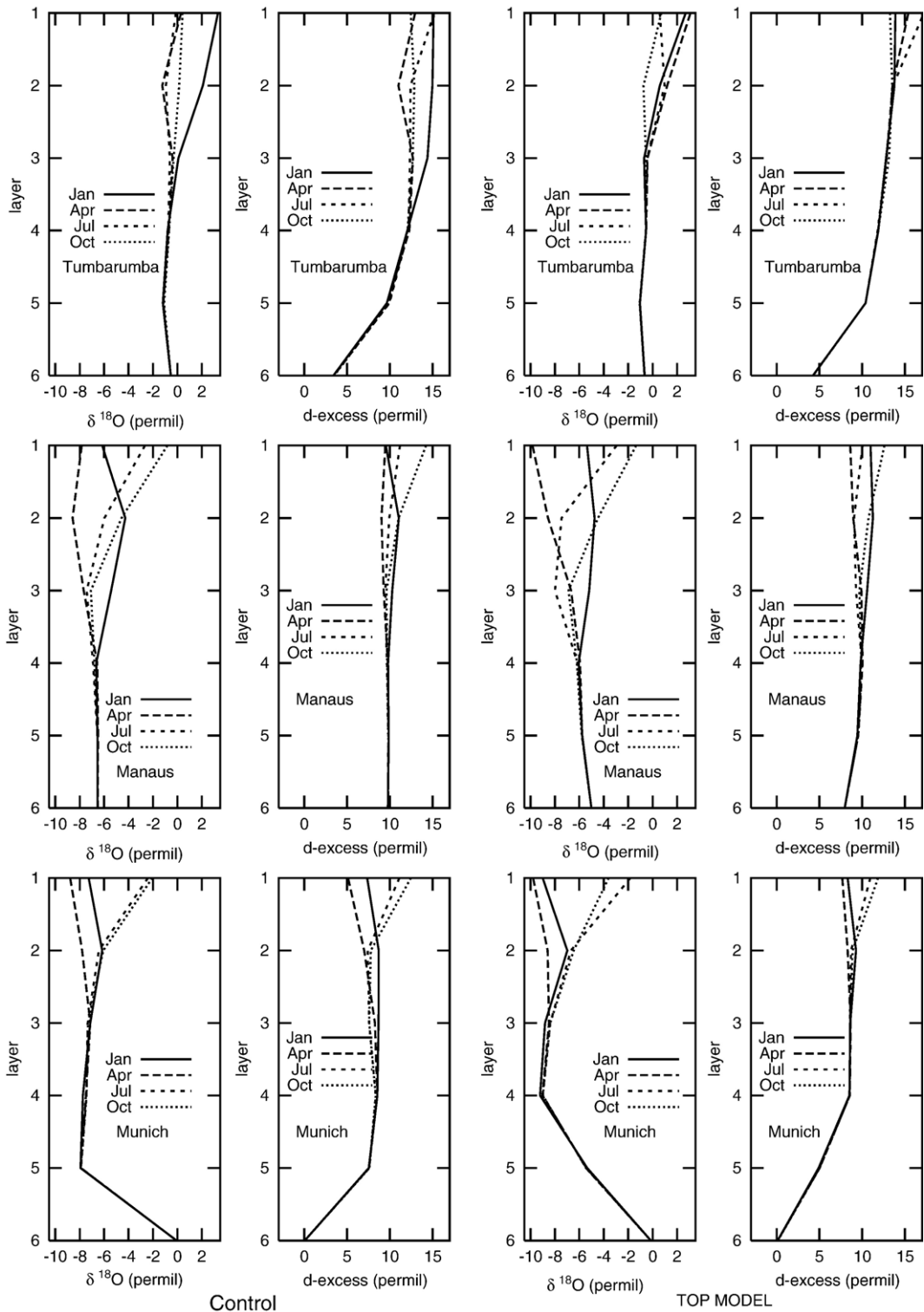


Fig. 5. Vertical soil profile of $\delta^{18}O$ ‰ and d-excess ‰. The graphs present the monthly means for January, April, July and October for year 20.

Table 3

Total river outflow and corresponding $\delta^{18}\text{O}$ ‰ for river basins containing investigated regions. The results of simulations are given for both control simulation and the simulation with TOPMODEL runoff

Basin	Outflow (km^3/month)	Obs. Outflow (km^3/month)	$\delta^{18}\text{O}$ (‰)	Obs. $\delta^{18}\text{O}$ (‰)
Murray	8.5/7.5	1.8	-1.3/-2.5	-1 to -5
Amazon	282.8/294.4	525.1	-6.5/-7.2	-4 to -7
Danube	14.1/11.4	17.1	-9.1/-10.2	~-10

we have correct separation of precipitation water into evaporation, transpiration and runoff.

5. Transient simulation

In order to assess the connection between the isotopic fields and the overall climate variability we examine the covariance of the fields in a specific transient simulation. This is drawn from an AMIP-style simulation, which used observed and reconstructed SST and sea ice fields from 1880 to 2000 to force the model. Additionally we also include appropriate radiative forcings (well mixed greenhouse gases, O_3 , solar, volcanic, aerosols (direct and indirect effects), land use change, etc.) as described in Hansen et al. (2005). We highlight the changes in land surface hydrology over a 90-year period 1900–1909 to 1990–1999. This allows for a 20-year period in which the soil isotope fields can equilibrate in accordance with what was seen in the previous section. Some residual effects in the deep layers may still be visible in some diagnostics. We note that with only a single run (not an ensemble), we are unable to distinguish decadal intrinsic variability (which is however relatively small) or the response to single forcings (such as land-use changes). Nonetheless, the correspondence of the climate fields to the isotope fields is relatively clear, and from sensitivity studies (not shown) appears to be a robust feature.

Given the lack of long historical isotope records (except through sparse paleoclimatic records) it is impossible to directly validate the long term isotopic changes seen in these simulations. Therefore we present the results in order to demonstrate the sensitivity of the isotope fields to larger scale changes and highlight potential regions and diagnostics that might be usefully monitored for signs of ongoing climate change. Such signs for instance of Amazon deforestation have already been proposed for isotopic modeling (McGuffie and Henderson-Sellers, 2004).

Firstly, we look at the precipitation, soil moisture and surface air temperature changes to determine the

base climate changes that occurred in the simulation (Fig. 6). We note that integrated fields such as the global mean surface air temperature have a good match to the historical observations, but regionally trends in the model will diverge from observed as a function of internal variability, potentially inaccurate regional forcings (particular aerosols) or poor representation of physics in the models themselves. However, since our goal here is to examine how the isotope changes are related to the climate changes within the context of the model, these departures from the observations are less of a concern. We will focus also on the regional changes in the areas that were diagnosed in the previous section, i.e. Europe, Amazonia and Australia.

There is significant global warming of about 0.6°C . Regionally, warming can be greater (around 1° over most continental areas), although some areas have very small warmings, most likely as a function of local aerosol forcings or dynamical effects. Polar warming is enhanced compared to the global mean due to basic ice-albedo feedback effects, but also because of the effect of black carbon (soot) on snow albedo (Hansen and Nazarenko, 2004). Generally, surface relative humidity increases in mid latitudes, and decreases in the tropical subsidence zones (not shown). In Australia humidity and rainfall increase while Amazon humidity and precipitation decrease. Soil wetness generally follows the rainfall trends.

In Asia, Indian rainfall decreases, while Chinese rainfall increases—consistent with a predominantly sea surface temperature forced response. In Africa, there is an overall decrease in precipitation, while in Europe, no consistent pattern is seen. River runoff patterns are consistent with the precipitation changes, for instance, giving a 15% decrease in total Amazon outflow.

In the corresponding isotopic fields, we look, in particular, at the isotopic ratio in precipitation, soil moisture and river runoff. While the areas that undergo significant change in the base climate variables also show up in the isotopic fields, there are large differences in the isotopic sensitivity in different regions. In particular, temperature and isotopes are proportional in the mid- to high-latitudes, but in the tropics, the isotopic sensitivity is mainly to precipitation (in the opposite sense) in accord with the classical ‘amount’ effect (Dansgaard, 1964). Specifically shifts in precipitation bands around the Inter-Tropical Convergence Zone (ITCZ) produce positive isotopic anomalies in regions of reduced precipitation, and vice versa.

The response is a little muted in the more integrated quantities such as soil moisture and runoff. However,

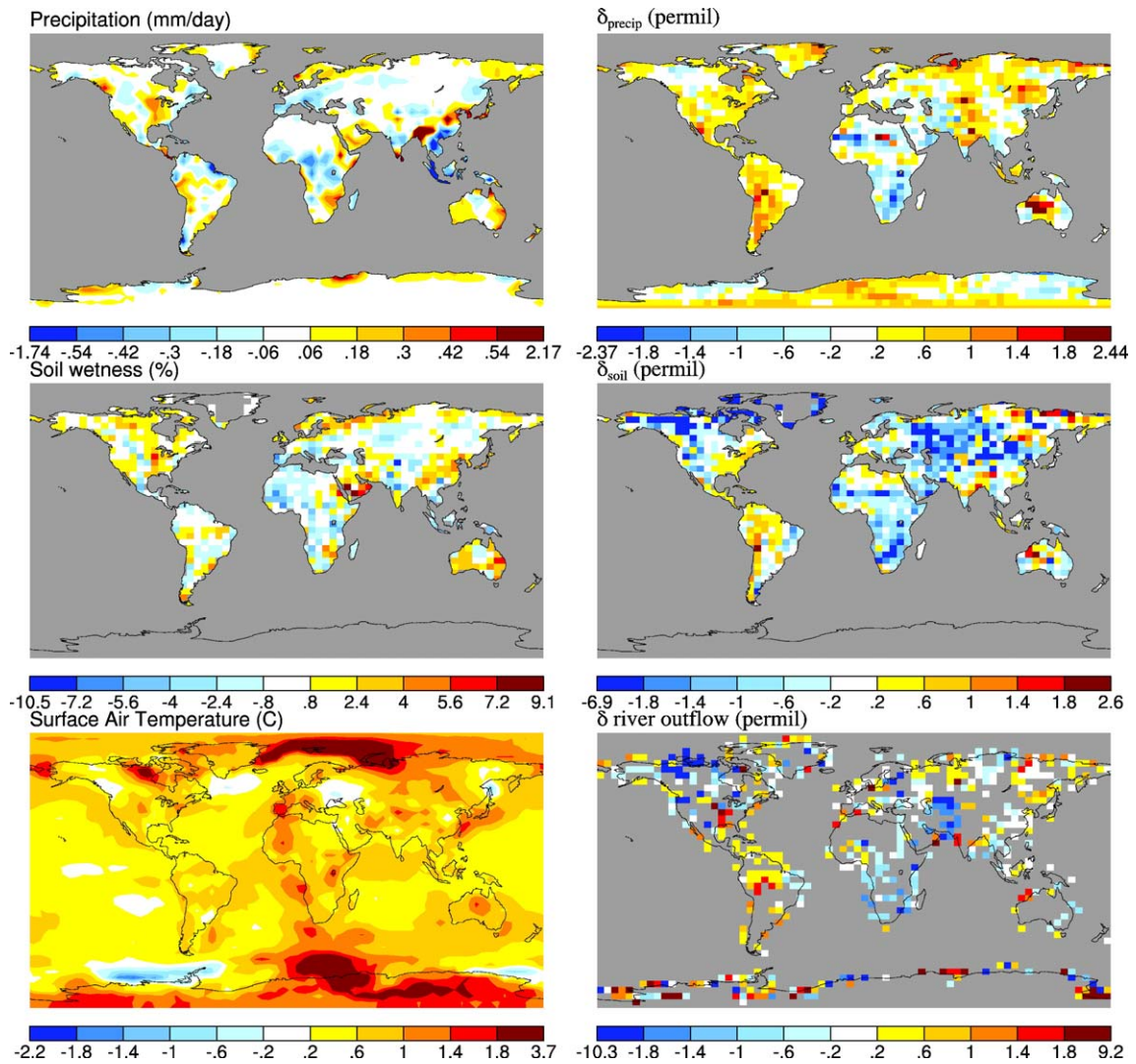


Fig. 6. Changes in precipitation, soil wetness, surface air temperature and the isotopic composition of $\delta^{18}\text{O}\text{‰}$ for precipitation, total soil water and river outflow over the period 1900–1909 to 1990–1999 in one transient AMIP simulation with radiative forcings included. River outflow data is presented for the cells which receive corresponding river water, hence some of the ocean cells near a river mouth also contain these data.

signals are still seen in the river outflow to the oceans, even though they integrate over large watersheds. These signals are a combination of the precipitation and runoff signals combined with changes in evaporation during the passage to the ocean.

In high northern latitudes, there is a significant difference in the trends for isotopic ratios in soil compared to precipitation. This is due to the existence of permanently frozen water in the deep soil layers. In areas where this occurs, there is no opportunity for the deeper layers to equilibrate with the infiltrating water, and as in the Munich case discussed in the previous section, the effective spin-up time is very long (if not infinite). However, as the climate warms the ice melts

and the soil moisture can equilibrate normally (which makes the soil water more depleted, and which shows up as strong negative changes in the figure).

Seasonally, DJF northern hemisphere precipitation changes are larger than the annual mean (not shown), but such effects are considerably damped in the total soil water or river runoff changes. Depending on how the seasonal cycle penetrates the soil in any particular location, this may be important in interpretation of specific paleo-proxies such as speleothems.

We also look specifically at the interannual changes at the three sites discussed in the previous section (Fig. 7). In the case of Manaus and Munich the difference between $\delta^{18}\text{O}_{\text{precip}}$ and $\delta^{18}\text{O}_{\text{soil}}$ takes between

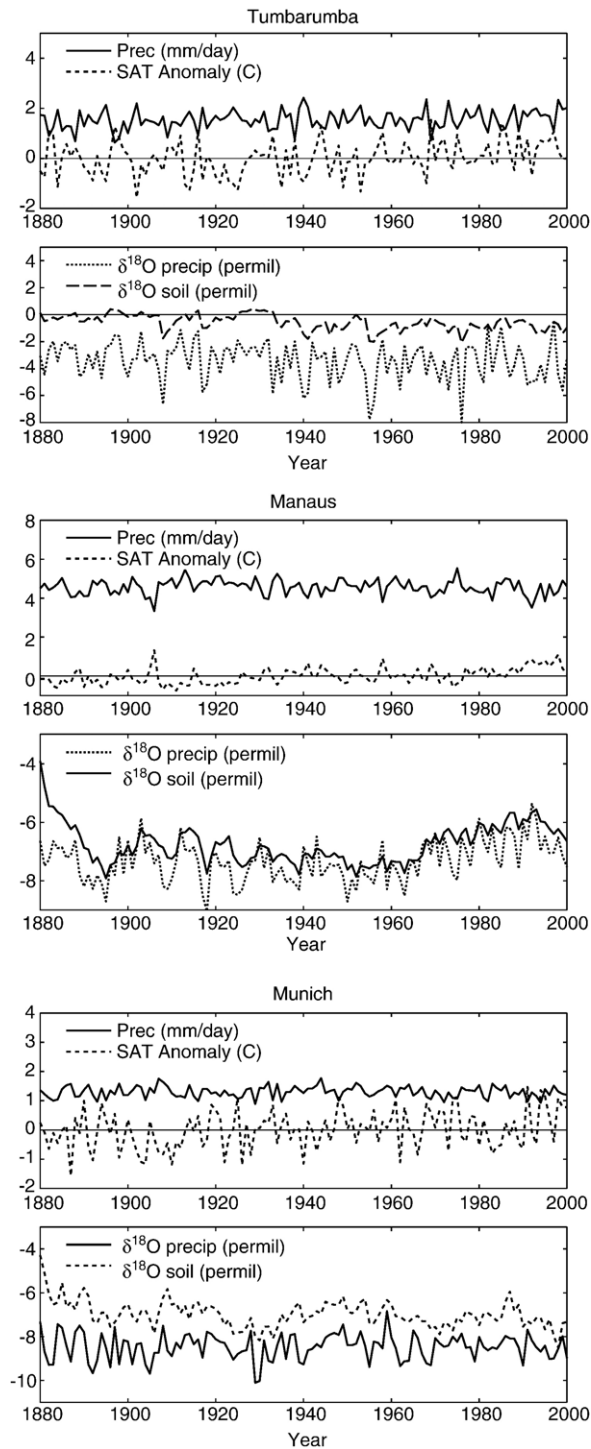


Fig. 7. Transient (annual mean) response of precipitation, surface air temperature, $\delta^{18}\text{O}_{\text{precip}}$ and $\delta^{18}\text{O}_{\text{soil}}$ at three highlighted sites over 120 years.

10 and 20 years to stabilize (in line with the spin up time estimates derived earlier). In Tumarumba, this is not seen, implying that the deepest layer likely never participates in the variability. In all three cases, the soil water isotopes exhibit strong coherence with the variations in the isotopes in precipitation, but with a small amount of damping and lag. The difference between the isotope ratios in the precipitation and the soil water indicate (as expected) that transpiration is the biggest term in Manaus and a smaller fraction of the total evaporation in Munich and Tumarumba. On an interannual basis the correlations between the amount of precipitation and its isotopic composition are -0.34 , 0.05 and -0.42 at Manaus, Munich and Tumarumba, respectively, indicating the importance of the amount effect in Manaus and Tumarumba in particular. Correlations with temperature are always positive 0.35 , 0.19 and 0.30 , respectively. Trends over the 100-year period 1900–2000 are significant only in Manaus where there is a decrease in precipitation and an increase in the isotopic content (by about 0.8‰) qualitatively consistent with observational studies (Henderson-Sellers et al., 2002).

In future studies with more ensemble members, we hope to be able to discern the isotopic patterns associated with ENSO and other patterns of climate variability and pin down what aspects of climate change may be reflected in the soil water and runoff isotopes.

6. Conclusions

We present results from the LSM of the GISS ModelE fitted with water isotope tracers. From the analysis here and in previous publications (Schmidt et al., 2005), this model has demonstrated some skill in modeling the climatology particularly of the isotopic ratios in precipitation and river runoff. However, in order for more specific tests and validation of the LSM to be performed, significantly more data is likely to be needed. Specifically, long time-series, such as exist already for some rivers, and multi-layer snapshots through the soil column will be required. However, while single site datasets can be useful for validating the land surface component itself, they are less useful for validating the GCM as a whole because of the difficulty in resolving processes at the grid box scale and smaller.

As shown here, the penetration of the seasonal cycle through depth and the degree to which fractionating evaporation occurs (as opposed to evapotranspiration) affect the isotope signals seen in rivers and might be expected to affect soil water proxies like speleothems. Thus continued validation of more sophisticated LSMs

is warranted as opposed to simply retaining a bucket scheme for isotope mass conservation. In particular, we demonstrate that the seasonal penetration and spin-up time for the LSM is dependent on whether we use a traditional or TOPMODEL-like calculation of the underground runoff, however which formulation is better is difficult to determine in the absence of more comprehensive observations. The isotopic analysis has also been useful in identifying a potential issue in our scheme related to deep soil layers that do not participate in water exchange. This will be examined in further analysis.

Acknowledgments

Climate model development at GISS is supported by NASA. Support for IA was partially provided by DOE grant DE-FG02-02ER63444. Development of the isotope modules was partly supported by NSF OCE-99-05038.

References

- Abramopoulos, F., Rosenzweig, C., Choudhury, B., 1988. Improved ground hydrology calculations for global climate models (GCMs): Soil water movement and evapotranspiration. *J. Climate* 1, 921–941.
- Beven, K.J., Kirkby, M.J., 1979. A physically-based variable contributing area model of basin hydrology. *Hydrol. Sci. J.* 24, 43–69.
- Dansgaard, W., 1964. Stable isotopes in precipitation. *Tellus* 16, 436–468.
- Friend, A.D., Kiang, N.Y., 2005. Land surface model development for the GISS GCM: effects of improved canopy physiology on simulated climate. *J. Climate* 18, 2883–2902.
- Gibson, J.J., Aggarwal, P., Hogan, J., Kendall, C., Martinelli, L., Stichler, W., Rank, D., Goni, I., Choudhry, M., Gat, J., Bhattacharya, S., Sugimoto, A., Fekete, B., Pietroniro, A., Maurer, T., Panarello, H., Stone, D., Seyler, P., Maurice-Bourgoin, L., Herczeg, A., 2002. Isotope studies in large river basins: a new global research focus. *EOS* 83 (52), 616–617.
- Hansen, J., Nazarenko, L., 2004. Soot climate forcing via snow and ice albedos. *Proc. Natl. Acad. Sci.* 101, 423–428. doi:10.1073/pnas.2237157100.
- Hansen, J., Sato, M., Ruedy, R., Nazarenko, L., Lacis, A., Schmidt, G.A., Russell, G., Aleinov, I., Bauer, M., Bauer, S., Bell, N., Cairns, B., Canuto, V., Chandler, M., Cheng, Y., Del Genio, A., Faluvegi, G., Fleming, E., Friend, A., Hall, T., Jackman, C., Kelley, M., Kiang, N., Koch, D., Lean, J., Lerner, J., Lo, K., Menon, S., Miller, R.L., Minnis, P., Novakov, T., Oinas, V., Perlwitz, J., Perlwitz, J., Rind, D., Romanou, A., Shindell, D., Stone, P., Sun, S., Tausnev, N., Thresher, D., Wielicki, B., Wong, T., Yao, M., Zhang, S., 2005. Efficacy of climate forcings. *J. Geophys. Res.* 110, D18104. doi:10.1029/2005JD005776.
- Henderson-Sellers, A., McGuffie, K., Zhang, H., 2002. Stable isotopes as validation tools for Global Climate Model predictions of the impact of Amazonian deforestation. *J. Climate* 15, 2664–2677.
- Henderson-Sellers, A., Fischer, M., Aleinov, I., McGuffie, K., Riley, W.J., Schmidt, G.A., Sturm, K., Yoshimura, K., Irannejad, P., 2006. Stable water isotope simulation by current landsurface schemes: results of iPILPS phase 1. *Glob. Planet. Change* 51, 34–58 (this volume).
- IAEA, J., 2001. GNIP maps and animations. International Atomic Energy Agency, Vienna. <http://isohis.iaea.org>.
- Jouzel, J., Koster, R.D., Suozzo, R.J., Russell, G.L., White, J.W.C., Broecker, W.S., 1991. Simulations of HDO and H₂¹⁸O atmospheric cycles using the NASA GISS general circulation model: Sensitivity experiments for present-day conditions. *J. Geophys. Res.* 96, 7495–7507.
- Lynch-Stieglitz, M., 1994. The development and validation of a simple snow model for the GISS GCM. *J. Climate* 7, 1842–1855.
- Matthews, E., 1983. Global vegetation and land use: New high-resolution data bases for climate studies. *J. Clim. Appl. Meteorol.* 22, 475–487.
- Matthews, E., 1984. Prescription of land-surface boundary conditions in GISS GCM: II. A simple method based on high-resolution vegetation data bases. NASA Tech. Memo. 86096, 1–20.
- McGuffie, K., Henderson-Sellers, A., 2004. Stable water isotope characterization of human and natural impacts on land-atmosphere exchanges in the Amazon Basin. *J. Geophys. Res.* 109, D17104.
- Milliman, J.D., Meade, R.H., 1983. World-wide delivery of river sediment to the oceans. *J. Geol.* 91, 1–21.
- Roesch, A., Wild, M., Gilgen, H., Ohmura, A., 2001. A new snow cover fraction parametrization for the ECHAM4 GCM. *Clim. Dyn.* 17, 933–946.
- Rosenzweig, C., Abramopoulos, F., 1997. Land-surface model development for the GISS GCM. *J. Climate* 10, 2040–2056.
- Schmidt, G.A., Hoffmann, G., Shindell, D.T., Hu, Y., 2005. Modelling atmospheric stable water isotopes and the potential for constraining cloud processes and stratosphere-troposphere water exchange. *J. Geophys. Res.* 110, D21314. doi:10.1029/2005JD005790.
- Schmidt, G.A., Ruedy, R., Hansen, J.E., Aleinov, I., Bell, N., Bauer, M., Bauer, S., Cairns, B., Canuto, V., Cheng, Y., Del Genio, A., Faluvegi, G., Friend, A.D., Hall, T.M., Hu, Y., Kelley, M., Kiang, N.Y., Koch, D., Lacis, A.A., Lerner, J., Lo, K.K., Miller, R.L., Nazarenko, L., Oinas, V., Perlwitz, J., Perlwitz, J., Rind, D., Romanou, A., Russell, G.L., Sato, M., Shindell, D.T., Stone, P. H., Sun, S., Tausnev, N., Thresher, D., Yao, M.-S., 2006. Present day atmospheric simulations using GISS ModelE: Comparison to in-situ, satellite and reanalysis data. *J. Climate* 19, 153–192. doi:10.1175/JCLI3612.1.
- Simpson, H.J., Herczeg, A.L., 1991. Stable isotopes as an indicator of evaporation in the river Murray, Australia. *Water Resour. Res.* 27, 1925–1935.
- Stichler, W., Schotterer, U., 2000. From accumulation to discharge: modification of stable isotopes during glacial and post-glacial processes. *Hydrol. Process.* 14, 1423–1438.
- Webb, R.S., Rosenzweig, C., Levine, E.R., 1991. A global data set of soil particle size properties. NASA Tech. Memo. 4286, 1–33.
- Webb, R.S., Rosenzweig, C., Levine, E.R., 1993. Specifying land-surface characteristics in general circulation models: Soil profile data set and derived water-holding capacities. *Glob. Biogeochem. Cycles* 7, 97–108.
- Zobler, L., 1986. A world soil file for global climate modeling. NASA Tech. Memo. 87802, 1–32.